https://doi.org/10.5194/acp-2022-133
Preprint. Discussion started: 23 March 2022

Atmospheric Chemistry and Physics Discussions

Cluster-based characterization of multi-dimensional tropospheric ozone variability in coastal regions: an analysis of lidar measurements and model results

Claudia Bernier[1], Yuxuan Wang[1], Guillaume Gronoff[2,3], Timothy Berkoff[2], K. Emma Knowland[4,5], John T. Sullivan[4], Ruben Delgado[6,7], Vanessa Caicedo[6,7], Brian Carroll[2,6]

[1] Department of Earth and Atmospheric Science, University of Houston, Houston, Texas, USA

[2] NASA Langley Research Center, Hampton, VA, 23666, USA

[3] Science Systems and Application Inc., Hampton, VA, 23666, USA

[4] NASA Goddard Space Flight Center, Global Modeling and Assimilation Office, Greenbelt, MD, 20771, USA

[5] Morgan State University, Goddard Earth Science Technology & Research (GESTAR) II, Baltimore, Maryland, USA

[6] Joint Center for Earth Systems Technology, Baltimore, MD, USA

[7] University of Maryland Baltimore County, Baltimore, MD, USA

Correspondence: Yuxuan Wang (ywang246@central.uh.edu)

Abstract. Coastal regions are susceptible to multiple complex dynamic and chemical mechanisms and emission sources that lead to frequently observed large tropospheric ozone variations. These large ozone variations occur on a meso-scale which have proven to be arduous to simulate using chemical transport models (CTMs). We present a clustering analysis of multi-dimensional measurements from ozone Light Detection And Ranging (LiDAR) in conjunction with both an offline GEOS-Chem CTM simulation and the online GEOS-Chem simulation GEOS-CF, to investigate the vertical and temporal variability of coastal ozone during three recent air quality campaigns: 2017 Ozone Water-Land Environmental Transition Study (OWLETS) 1, 2018 OWLETS 2, and 2018 Long Island Sound Tropospheric Ozone Study (LISTOS). We developed and tested a clustering method that resulted in 5 ozone profile curtain clusters. The established 5 clusters all varied significantly in ozone magnitude vertically and temporally which allowed us to characterize the coastal ozone behavior. The lidar clusters provided a simplified way to evaluate the two CTMs for their performance of diverse coastal ozone cases. The two models have fair-to-good relationships with the lidar observations (R = 0.66 to 0.69) in the low-level altitude range (0 to 2000 m), with low and unsystematic bias for GEOS-Chem and high systemically positive bias for GEOS-CF. In the mid-level altitude range (2000 to 4000 m), both models have difficulty simulating the vertical extent and variability of ozone concentrations in all 5 clusters, with a weak relationship with the lidar observations (R = 0.12 and 0.22, respectively). GEOS-Chem revealed a high systematic negative bias and GEOS-CF an overall low unsystematic bias range. Using ozone vertical and diurnal distribution from lidar measurements, this work provides new insights on model's proficiency in complex coastal regions.

https://doi.org/10.5194/acp-2022-133
Preprint. Discussion started: 23 March 2022


Atmospheric Chemistry and Physics Discussions

1. Introduction

Tropospheric ozone (O_3) is an important secondary pollutant created by multiple reactions involving sunlight, nitrogen oxides (NO_x = NO + NO_2), and volatile organic compounds (VOCs) which, in accumulation, can have damaging effects on human and plant health. In addition to its photochemical growth, O_3 can easily be influenced by local and regional transport mechanisms. For coastal regions, surface O_3 is highly variable in time and space due to its susceptibility to many factors such as local ship emissions, long range transport, and sea/bay breeze processes. Multiple studies have proven the strong influence that sea/bay breeze and wind flow patterns can have on the accumulation of coastal O_3 and can often lead to poor air quality (e.g., Tucker et al., 2010; Martins et al., 2012; Stauffer et al., 2012; Li et al., 2020). Loughner et al. (2014) highlighted the importance for understanding the ability for bay breeze events to cause O_3 differences not only spatially but vertically in coastal regions.

This variability is challenging for air quality models to capture as high-resolution measurements are necessary to fully understand and simulate this O_3 behavior in coastal regions. For example, Dreessen et al. (2019) tested the U.S. Environmental Protection Agency (EPA) Community Multiscale Air Quality (CMAQ) model's ability, configured at 12 km, to simulate O_3 exceedances at Hart Miller Island in Maryland (HMI) revealing high bias and 'false alarms' due to several reasons such as emission transport over water and the coarse model resolution's inability to capture fine-scale meteorology and transport. Cases such as sea/bay breeze events, which directly contribute to high coastal O_3 cases, are denoted by local meteorological mechanisms such as surface wind speed deceleration, wind direction convergence and recirculation (Banta et al., 2005). Air quality models with coarse horizontal and vertical resolutions are not able to capture such fine developments (Caicedo et al., 2019). Ring et al. (2018) also used CMAQ to estimate the impact of ship emissions on the air quality in eastern U.S. coastal regions indicating that an understanding of the vertical profiles of emissions was significant for improving air quality simulations. These are consistent and unanimous issues with air quality modeling in coastal regions. Since offshore sites within coastal regions are historically under sampled due to the difficulty of water-based measurements, this problem is still pertinent today.

Recently, three associated air quality campaigns set out to address this issue (https://www-air.larc.nasa.gov/index.html): 2017 & 2018 NASA Ozone Water-Land Environmental Transition Study (OWLETS - 1 & OWLETS - 2) and Long Island Sound Tropospheric Ozone Study (LISTOS), set out to address this issue (e.g., Sullivan et al., 2019). These three campaigns were each conducted in highly populated coastal regions along the Chesapeake Bay in Virginia and Maryland and Long Island Sound in the New England/Middle Atlantic region, respectively, that are vulnerable to O_3 exceedances with the goal of filling the measurement gaps in these regions. During these campaigns, a suite of detailed airborne and ground measurements were taken during the course of highly polluted summer months (end of May through August) to capture the variability of pollutants, including O_3 and its precursor species, and the distinct meteorological processes specific to land-water regions that affect them.

The three campaigns strategically placed multi-dimensional tropospheric lidar measurements of O_3 on and offshore in order to capture critical land-water gradients and to fill the deficit of measurements in these under monitored areas. These measurements were supported as part of NASA's Tropospheric Ozone Lidar Network (TOLNet). Continuous profile

https://doi.org/10.5194/acp-2022-133
Preprint. Discussion started: 23 March 2022


Atmospheric Chemistry and Physics Discussions

measurements from O_3 lidars highlight important regional transport and temporal variations of O_3 in the lower and middle levels of the troposphere that are usually difficult to capture by most satellite-based remote-sensing instruments (Thompson et al., 2014). Lidar measurements are unique in their ability to capture high resolution full O_3 2-D profile curtains over a period of time that indicate pollutant transport and can help in understanding O_3 behavior in coastal regions. In Gronoff et al. (2019), the co-located lidar at the Chesapeake Bay Tunnel Bridge (CBBT) during OWLETS-1 successfully captured a near-surface maritime ship plume emission event on August 01, 2017. An ensemble of other instruments (e.g., drones, Pandora spectrometer systems, etc.) launched near the shipping channel captured elevated NO_2 concentrations while the lidar instrument captured a depletion of O_3 simultaneously. The lidar was able to capture the unique low range altitude O_3 concentrations which elucidated the evolution of the trace-gas concentrations during this ship plume event.

Several studies have thoroughly evaluated the results from the air quality campaigns used in this study but were focused more on specific case studies (Dacic et al., 2019; Sullivan et al., 2019; Gronoff et al., 2019). Dacic et al. (2019) used lidar measurements of a high O_3 episode during OWLETS-1 to evaluate the ability of two NASA coupled chemistry-meteorology models (CCMMs), the GEOS Composition Forecast ("GEOS-CF"; Keller et al., 2021) and MERRA2-GMI (Strode et al., 2019), to simulate this high O_3 event. They found that the GEOS-CF model performed fairly in simulating O_3 in the lower level (between 400 to 2000 m ASL) and outperformed MERRA2-GMI based on surface observations at multiple monitoring sites and by a median difference of -6 to 8 % +/- 7 % at both lidar sites. In the case of this event, GEOS-CF was able to simulate the 2-D O_3 profile curtains at small scales. At the time of the Dacic et al. (2019) study, only processed observational data from OWLETS-1 was available.

For this study, we took advantage of 91 captured 2-D (vertical and diurnal) O_3 curtain profiles from all three air quality campaigns (Sect. 2). To characterize the different behaviors of O_3 in coastal regions, we developed a novel clustering method based on the altitude and time dimensions of the lidar measurements that organized the profile curtains (Sect. 2). We used the developed clusters to evaluate the ability of both offline and online GEOS-Chem and GEOS-CF simulations to reproduce the coastal O_3 and wind characteristics highlighted by each cluster (Sect. 3).

2. Materials & Method

2.1. Air quality campaigns

During the years 2017 and 2018, NASA in partnership with other U.S. national agencies and university research groups orchestrated three air quality campaign studies that focused on key land and water observations: OWLETS-1, OWLETS-2, and LISTOS. OWLETS-1 was conducted in 2017 from July 5 to August 3, while OWLETS-2 and LISTOS were conducted in 2018 from June 6 to July 6 and July 12 to August 29, respectively. All campaigns took advantage of a multitude of ground, aircraft, and remote sensing measurements. For the sake of this study, we will focus on measurements from the two lidars from the TOLNet: NASA Langley Mobile Ozone Lidar (LMOL) (De Young et al. 2017; Farris et al. 2018; Gronoff et al, 2019, 2021) and NASA Goddard Space Flight Center (GSFC) Tropospheric Ozone (TROPOZ) Differential Absorption Lidar (DIAL) (Sullivan et al. 2014, 2015a), which ran simultaneously at the marked positions in Figure 1. The TOLNet data from all three

https://doi.org/10.5194/acp-2022-133
Preprint. Discussion started: 23 March 2022

Atmospheric Chemistry and Physics Discussions

campaigns are available on the NASA LaRC Airborne Science Data for Atmospheric Composition archive (https://www-air.larc.nasa.gov/missions.htm; accessed – 20 January 2021).

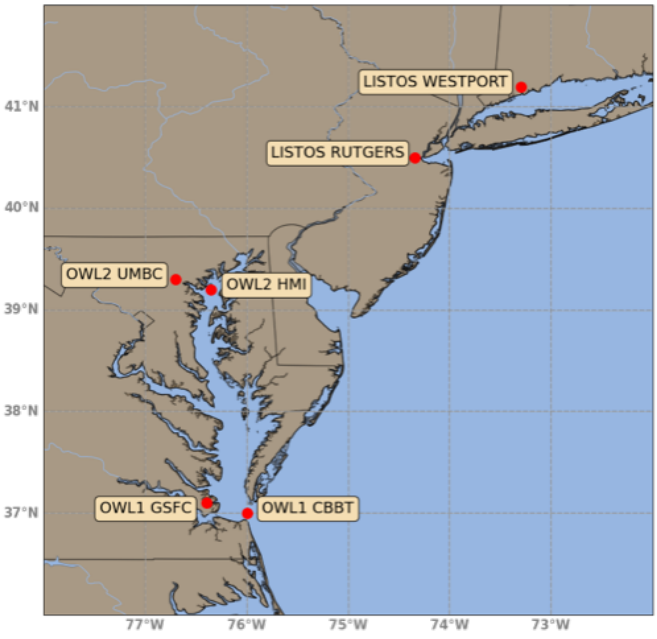

Figure 1. An inset map of the Chesapeake Bay airshed in Maryland, Virginia, and Long Island Sound in New York with the six lidar monitoring locations used for OWLETS-1, OWLETS-2, and LISTOS highlighted and labeled.

The two lidars were placed strategically for each campaign (Figure 1), so that one lidar was closest to over-water measurements while the other was farther inland with the goal of examining how O_3 transport and concentration is influenced by specific coastal mechanisms such as the land–water breezes. For OWLETS-1, the LMOL lidar was used at the CBBT [37.0366°N, 76.0767°W], depicting the real time over water O_3 measurements while the GSFC TROPOZ lidar was stationed at NASA Langley Center [37.1024°N, 76.3929°W] further inland. Similarly, for OWLETS-2, the LMOL lidar was stationed for the over water measurements at Hart Miller Island [39.2449° N, 76.3583° W] and GSFC TROPOZ was stationed at the University of Maryland, Baltimore County (UMBC) [39.2557° N, 76.7111° W]. Finally, for LISTOS, LMOL was at the Westport site [41.1415° N, 73.3579° W] and TROPOZ at Rutgers [40.2823° N, 74.2525° W]. For the sake of this study the unique benefits due to the different placements (onshore versus offshore) of the co-located lidars are not specifically evaluated. Instead, the study focuses on the benefits of detailed and multi-dimensionality of both lidar instrument data in general.

Routine lidar measurements were taken for the duration of the campaigns providing 91 multi-dimensional O_3 profile curtains. Both lidars retrieve data at a 5-min temporal resolution and use a common processing scheme to produce a final O_3 product which was used for this study. In this study, the individual profile curtains refer to the "full day", vertical and diurnal

https://doi.org/10.5194/acp-2022-133
Preprint. Discussion started: 23 March 2022


Atmospheric Chemistry and Physics Discussions

lidar measurements. In this study, 91 individual 2-D profile curtains were used from both lidars from the three campaigns: 26 profile curtains from OWLETS-1, 28 profile curtains from OWLETS-2, and 37 profile curtains from LISTOS.

To evaluate meteorological impacts on the lidar O_3 clusters and distinguish certain model discrepancies we used various temperature and wind measurements. Hourly observed temperature, wind speed, and wind direction from surface monitors pertaining to the study area were obtained from the Air Quality System (AQS) (data can be accessed at https://aqs.epa.gov/aqsweb/airdata/). Along with the O_3 lidar instruments, we utilized high resolution vertical and horizontal wind speed and direction data monitored by Doppler wind lidar Leosphere WINDCUBE 200s instruments deployed at HMI during OWLETS-2 during LISTOS (e.g., Couillard et al., 2021; Coggon et al., 2021; Wu et al., 2021).

2.2. Clustering lidar data

2.2.1 Description of the ozone lidar measurements

The lidar instrument is unique in that it provides high dimensional profile measurements of O_3, as opposed to one dimensional surface measurements from air quality monitoring sites. The two TOLNet lidars used during the campaigns have been evaluated for their accuracy during previous air quality campaigns (DISCOVER-AQ; https://www-air.larc.nasa.gov/missions/discover-aq and FRAPPÉ; https://www2.acom.ucar.edu/frappe) and have also been compared against each other (e.g., Sullivan et al., 2015; Wang et al., 2017). The two lidars have different transmitter and retrieval components but produce O_3 profiles within 10 % of each other as well as compared to ozonesondes (Sullivan et al., 2015). In comparison with other in situ instrument measurements, the TOLNet lidars were found to have an accuracy better than ±15 % for capturing high temporal tropospheric O_3 vertically proving their capability of capturing high temporal tropospheric O_3 variability (Wang et al., 2017; Leblanc et al., 2018).

To characterize coastal O_3 during the summer months, we use a multitude of lidar profile curtains obtained during the OWLETS 1, 2, and LISTOS campaigns. The two lidars used in the campaigns produced profile curtains of O_3 from 0 – 6000 m above ground level (AGL) with some days beginning as early as 06:00 local time (EDT) and ending measurements as late as the last hour of the day. One of the challenges is that the multiple lidar datasets are not always uniform; although most of the profile curtains began at or around 08:00 EDT, the lidar measurements commence and conclude at different times. At the time of these campaigns, the lidar data retrieval was constrained by the availability of personnel as well as the availability of electricity in remote areas (at time of writing, the lidar instrument systems have been updated and are now more fully automatized for use during succeeding campaigns removing such constraints). Due to this constraint, the 91 lidar curtains range from as short as a 6-hour window to a full 24-hour window. Similarly, the profile curtains do not have an exact uniform altitude range either. In the processing of the lidar data, some measurements may be filtered out and removed due to issues, such as clouds, which can influence and degrade the retrieval leaving some blocks of empty data within the vertical altitude dimension. When the cloud conditions are perfect, the limiting factor for the altitude is the solar background: the UV from the sun is a source of noise that prevents the detection of the low level of backscattered photons. For LMOL, this means that the maximum altitude is about 10 km AGL at night (Gronoff et al., 2021) and lowered to about 4 km AGL at solar noon (worse

https://doi.org/10.5194/acp-2022-133
Preprint. Discussion started: 23 March 2022


Atmospheric Chemistry and Physics Discussions

conditions possible for the summer in the continental U.S. resulting in below 4 km AGL). This results in a general scarcity of O_3 measurements above 4000 m AGL for most of the vertical profile curtains.

155 **2.2.2 Clustering approach and application**

To facilitate the comparison of the 2-D O_3 profile curtains and the air quality model simulations we used a cluster analysis that categorized the behavior of the tropospheric O_3 captured in the curtain profiles. Clustering methods are commonly used in air quality and atmospheric studies to group and characterize large datasets (Darby, 2005; Alonso et al., 2006; Christiansen, 2007; Davis et al., 2010; Stauffer et al., 2018). In our previous work, we have successfully used clustering methods to
160 automatically characterize diurnal patterns of surface winds and surface O_3 in the Houston-Galveston-Brazoria area that proved to perform better than a rudimentary quantile method to reveal the dependence of surface O_3 variability on local and synoptic circulation patterns on the Gulf Coast (Bernier et al., 2019; Li et al., 2020)

In evaluating the structure of the lidar measurements and working within measurement limitations (described in Sect. 2.2.1) from the three air quality campaigns, we developed a method to cluster multi-dimensional O_3 profile curtains using K-
165 Means clustering algorithm. Input features (seed values) were rationally established to best represent the behavior of O_3 temporally and vertically without including an excessive amount of input features, which can weaken the results of clustering. With the goal of evaluating lower level tropospheric O_3 and based on description of the structure and constraints of the lidar measurements, the features were tailored to the altitude range 0 – 4000 m AGL and time range of 06:00 EDT – 21:00 EDT.

Figure 2 illustrates the 8 features that represent slabs of altitude and time used in the cluster analysis. For each O_3 profile
170 curtain (total of 91), we calculated the average O_3 from the following time and altitude range: Features 1 – 4 altitudes range from 0 – 2000 m; Features 5 – 8 altitudes range from 2000 – 4000 m. The two altitude ranges were determined to best represent different O_3 transport events although they do not explicitly represent these layers. For Features 1 – 4, O_3 would most likely primarily be affected by local production and pollution transport while for Features 5 – 8, O_3 would more likely be associated with long range transport (e.g. interstate). As planetary boundary layer growth (PBL) in coastal regions do not usually reach
175 altitudes greater than 2000 m, mixing between the boundary layer and free troposphere would presumably take place within the low-level altitude bin. Additional attention to the PBL in the selecting of low versus mid-level features for the clustering will be investigated in future work. For clarity, we will use the terms low-level and mid-level features to address the two altitude subsets e.g., Features 1 – 4 and 5 – 8, respectively. Feature 1 and 5 time range from 06:00 – 08:00 EDT; Feature 2 and 6 from 08:00 – 12:00 EDT; Feature 3 and 7 from 12:00 – 16:00 EDT; and Feature 4 and 8 from 16:00 – 21:00 EDT. The four
180 subset time ranges were indicated to best represent features that characterize the common diurnal behavior of O_3.

https://doi.org/10.5194/acp-2022-133
Preprint. Discussion started: 23 March 2022

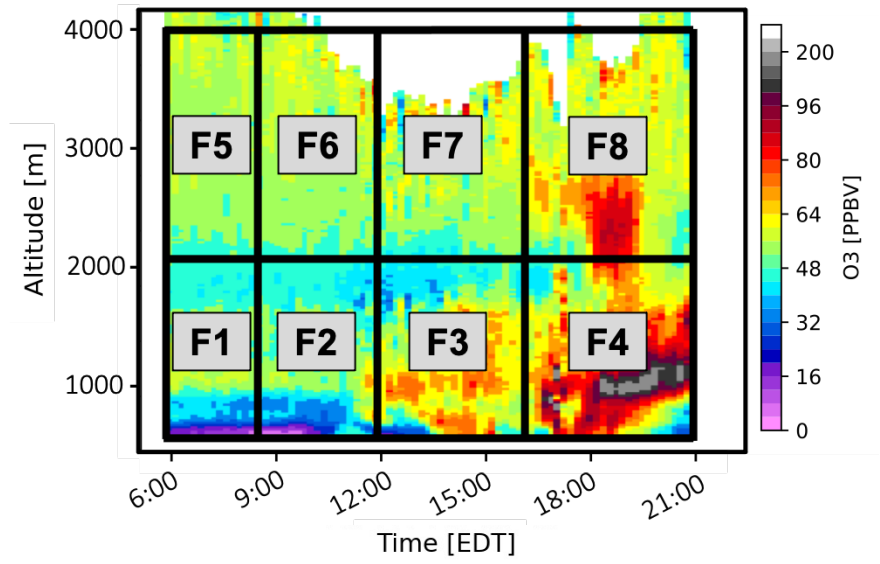

Figure 2. Clustering method developed for clustering vertical O_3 profiles taken from lidar measurements. The color coding shows a typical day of lidar measurements of O_3 profiles on August 6, 2018, from the LMOL at Westport, CT during the LISTOS Campaign. F1 – F8 indicate the time and altitude range of the eight features used for the clustering algorithm.

The features were evaluated for cluster tendency, essentially to confirm our dataset contained meaningful clusters. One statistical approach was used to test the dataset called Hopkins statistic which measures whether there is uniform distribution (spatial randomness) within the dataset (Lawson and Jurs, 1990). The results calculated using the Hopkins statistic concluded a value higher than 0.75 (actual = 0.77) which by this standard indicates a clustering tendency at the 90% confidence level. Evaluating different feature options did not lead to better statistical results than with the final chosen features. To visualize the cluster tendency of our dataset, we applied the algorithm of the visual assessment of cluster tendency (VAT) approach (Bezdek and Hathaway, 2002) which uses the Euclidean distance measure to compute the dissimilarity matrix in the dataset and creates an ordered dissimilarity matrix image. Figure S1 shows the VAT approach results which indicates high similarity (red) and low similarity (blue) and confirms a cluster structure (not random) within our dataset.

Since the choice of clustering algorithm is subjective, we chose K-means clustering for its simplicity and widespread use. To use the K-Means clustering algorithm, the optimal number of clusters based on your dataset must be chosen beforehand. For this study, the package Nbclust (Charrad et al., 2014) in R was used, which applies 30 indices for determining the optimal number of clusters. Using this package, as well as testing the quality of the clustering results using the silhouette method (Kaufman & Rousseeuw, 1990), we selected six clusters as the optimal number of clusters. Since the K-Means clustering algorithm is based on the Euclidean distance to each centroid, the input data was normalized (to a mean of zero and standard deviation of one) to ensure each feature is given the same importance in the clustering (Aksoy & Haralick, 2001; Larose,

https://doi.org/10.5194/acp-2022-133
Preprint. Discussion started: 23 March 2022


Atmospheric Chemistry and Physics Discussions

2005). The resulting six clusters (described fully in Sect. 3.1) represent clusters of regularly observed lidar O_3 curtains for the regions of our study during the campaign periods.

205

2.2.3 Missing data

Although the input features were tailored based on the structure of the lidar measurements, the remaining data still had missing data points. In performing a quick evaluation on the 8 input features (Figure S2), we found that Features 1, 4, 5, and 8 had the most missing data while Features 2, 3, 6, and 7 had few or zero cases of missing data. This means that the earlier 210 morning measurements (06:00 – 12:00 EDT) and the later evening measurements (16:00 – 21:00 EDT) had the most cases of missing data points. This is plausible as the campaign teams were best able to retrieve clear measurement during midday/evening hours (12:00 – 16:00 EDT). As a result, 51 out of 91 O_3 profile curtains had at least one missing data point (feature) throughout the individual profile curtain.

A common practice for dealing with missing data is complete case analysis (CCA), in which observations with missing 215 values are completely ignored, leaving only the complete data to cluster. CCA can be inefficient as it introduces selection bias since the sample data no longer retains the state of the original full dataset (Donders et al., 2006; Little & Rubin, 2014). When we applied CCA, there were only 40 O_3 profile curtains of complete data, removing over half of the study profiles. Instead, we used a more comprehensive solution – imputation - that yields unbiased results (Donders et al., 2006). For this study we used the single imputation (SI) technique *knnImputation* in R (Torgo, 2010), which uses the k-nearest neighbors and searches 220 for the most similar cases and uses the weighted average of the values of those neighbors to fill the missing data. Essentially, this method selects the days that have the most similar profile curtain to any profile which has missing data points and uses those real data points to calculate a weighted mean that will fill in the missing data. We acknowledge using an imputation method on the dataset will possibly introduce a bias which is difficult to quantify, but this allows the use of the full 91 profile curtains of O_3 data. The silhouette method was used to test the quality of the newly imputed dataset and proved to be no worse, 225 nor better, than the CCA (*real data*) results. Therefore, the dataset was first imputed using SI to create a complete dataset and then the clustering method described in the sect. before (2.2.2) was applied to the complete imputed dataset.

2.3. Model simulations

The offline GEOS-Chem chemical-transport model (CTM) was utilized to simulate the spatial and temporal variability 230 of coastal O_3 in the Chesapeake Bay and Long Island Sound during the time of the campaigns. The GEOS-Chem model is a global 3-D CTM driven by assimilated meteorological data from the NASA Global Modeling and Assimilation Office (GMAO). Our simulations were driven by reanalysis data from Modern-Era Retrospective analysis for Research and Applications, Version 2 (MERRA-2; Gelaro et al., 2017). We ran a nested GEOS-Chem (v12-09) simulation at 0.5° x 0.625° horizontal resolution over the eastern portion of North America and adjacent ocean (90 – 60°W, 20 – 50°N), using lateral 235 boundary conditions updated every three hours from a global simulation with 2° x 2.5° horizontal resolution. The nested GEOS-Chem simulation was run with 72 vertical levels from 1013 to 0.01 hPa. Since the study focuses on the altitude range

https://doi.org/10.5194/acp-2022-133
Preprint. Discussion started: 23 March 2022


Atmospheric Chemistry and Physics Discussions

0 – 4000 m, the first 20 vertical levels from GEOS-Chem were used with 14 levels within the boundary layer (≤ 2000 m). The nested simulation was conducted for the study periods June – September 2017 and April – August 2018. We used the standard "out-of-the-box" unmodified default settings from the tropospheric chemistry chemical mechanism (tropchem) with global anthropogenic emissions from the Community Emissions Data System (CEDS) inventory (McDuffie et al, 2020) and U.S. Environmental Protection Agency (EPA) National Emissions Inventory (NEI) 2011 for monthly mean North American regional emissions (EPA NEI, 2015).

We also used results from NASA's near real-time forecasting system, GEOS-CF, an online GEOS-Chem simulation (v12-0-1) from GMAO (https://gmao.gsfc.nasa.gov/-weather_prediction/GEOS-CF/) with GEOS coupled to the GEOS-Chem tropospheric-stratospheric unified chemistry extension (UCX) and run at a high spatial resolution of 0.25°, roughly 25 km (Keller et al., 2021, Knowland et al., 2021). The vertical resolution for GEOS-CF is interpolated onto 72 vertical levels from 1000 to 10 hPa. Since the study focuses on the altitude range 0 – 4000 m, the first 21 vertical levels from GEOS-CF were used with 14 levels within the boundary layer (≤ 2000 m). Prior to the launch of the 12z five-day forecast, GEOS-CF produces daily global, 3-D atmospheric composition distributions using the GEOS meteorological replay technique (Orbe et al., 2017), and this study makes use of these historical estimates, made available to the public for the period since January 2018. Therefore, the GEOS-CF results shown in this study only include the dates from OWLETS-2 and LISTOS campaigns, since they both occurred in 2018.

While both model simulations use similar versions of GEOS-Chem chemistry, there are noteworthy differences to keep in mind during the analysis of the clustering. The main differences between the two models are (1) GEOS-Chem is an offline CTM using archived meteorology, while GEOS-CF simulates atmospheric composition simultaneously with meteorology (online); (2) the spatial resolution of the GEOS-CF model (0.25°) is higher than GEOS-Chem (0.5° x 0.625°); and (3) the GEOS-CF model runs with Harmonized Gridded Air Pollution (HTAP; v2.2; base year 2010) anthropogenic emissions from the Emission Database for Global Atmospheric Research (EDGAR), while GEOS-Chem was run with CEDS anthropogenic emissions (base year 2014). These imperative differences can lead to disparities in the following results.

3. Results & Discussion

3.1 Overview of the 2-D O_3 curtain clusters

The clustering results reveal distinctive characterized O_3 behavior during the three campaigns in which O_3 concentrations vary significantly across the clusters. As previously mentioned in Sect. 2.2.3, the clustering analysis initially identified six cluster groups from the O_3 profile curtains. Only one date was assigned to Cluster 6 (16 June 2018): the lidar profile curtain on this day (Figure S3) shows a large fraction of data missing, and the available data have relatively high O_3 throughout the lowest 3 km, which is different from other clusters. Therefore, we consider Cluster 6 to be an outlier and will not include it in the subsequent analysis.

Various cluster statistics including maximum and minimum O_3 and surface meteorological factors for the remaining five clusters are summarized in Table 1. With only 5 of the 2-D profile curtains assigned, Cluster 5 depicts the least common O_3

https://doi.org/10.5194/acp-2022-133
Preprint. Discussion started: 23 March 2022

Atmospheric Chemistry and Physics Discussions

behavior during the campaigns. On the other hand, Cluster 3 is the most common O_3 behavior during the campaigns with 28 profile curtains assigned to this cluster. Following Cluster 3, Cluster 1 is the next most common cluster with 25 profile curtains. Cluster 2 and Cluster 4 fall in the middle of the pack with 14 and 18 profile curtains assigned to the cluster numbers, respectively.

Cluster (#)	**a) No. of vertical profiles**	**b) O_3 Max** (ppb)	**c) O_3 Min** (ppb)	**d) T** (°F)	**e) WS** (m s^{-1})
HMO (1)	25	86.50	42.17	73.80	1.51
LLO (2)	14	72.77	28.85	71.42	1.62
MCO (3)	28	86.64	34.18	77.34	1.30
HLO (4)	18	97.77	44.08	77.79	1.24
LMO (5)	5	67.70	29.07	74.93	1.51

Table 1. Lidar vertical O_3 profile cluster statistics: a) total number of vertical profiles; b) O_3 maximum; c) O_3 minimum O_3; d) AQS monitoring station cluster mean surface temperature and e) AQS monitoring station cluster mean surface wind speed. The statistics and averages were derived from the total number of vertical profiles assigned to each cluster.

The five clusters were distinguished by the varying O_3 concentrations between the low-level and mid-level as well as temporal variations. Figure 3 quantifies the between-cluster differences by separating the two altitude subsets for lucidity as the majority of the cluster differences are contrasted between the low and mid-level. In the low-level, all five clusters exhibit the common O_3 diurnal pattern where surface O_3 is titrated overnight and reaches a minimum but then is quickly exacerbated with the increase of sunlight throughout the day and typically peaks after midday. The extent of this common diurnal pattern varies by cluster.

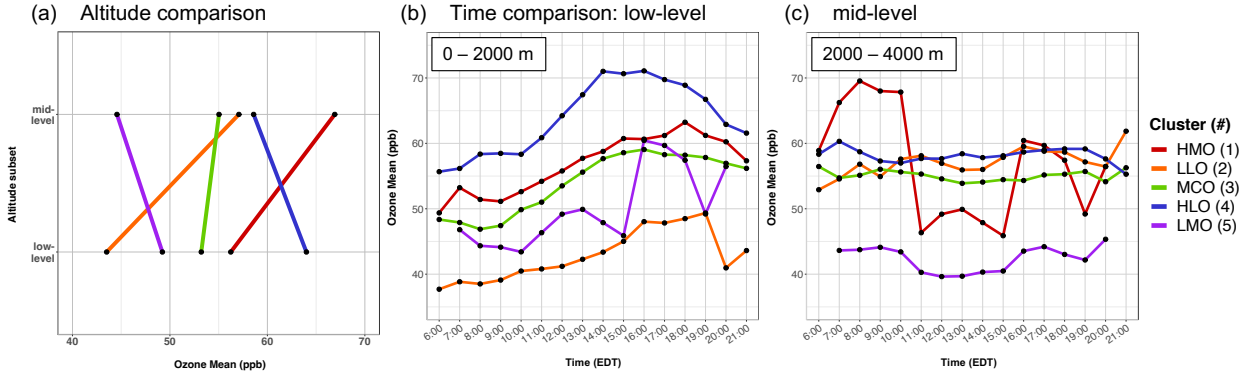

https://doi.org/10.5194/acp-2022-133
Preprint. Discussion started: 23 March 2022


Atmospheric Chemistry and Physics Discussions

295 **Figure 3.** Lidar cluster O_3 averages for the five clusters (depicted in colors). a) Mean O_3, averaged over time, comparison between the 2 altitude subsets (0 – 2000 m = low-level; 2000 – 4000 m = mid-level). Mean O_3, averaged over altitude, diurnal pattern comparison separated by b) low-level and c) mid-level.

Cluster 1 has the second highest low-level O_3 peak and the highest mid-level O_3 concentrations averaging at 67 ppb
300 (Figure 3a). Cluster 1 also exhibit the most unique pattern of mid-level O_3 (Figure 3c), with the highest concentrations found in the early morning and an uncharacteristic plunge to lower O_3 concentrations from 11:00 – 15:00 EDT. This is contrary to the other clusters which do not show as much O_3 magnitude variation temporally in the mid-level. In assessing the individual curtain profiles assigned to Cluster 1, the majority of the curtains reveal concentrated residual layers in the mid-level and early in the temporal profile that diffuse after the morning. This explains the uncharacteristic behavior of mid-level O_3 in Cluster 1.
305 Cluster 2 has the lowest low-level O_3 peak among the clusters averaging at 44 ppb (Figure 3a) with also the lowest morning O_3 (from 6:00 – 10:00 EDT) and moderate mid-level O_3 concentrations. Distinct from the other clusters that differ greatly in O_3 concentrations vertically, Cluster 3 has the most uniform vertical O_3 extent between the low and mid-level (Figure 3a). Cluster 4 reaches the highest low-level O_3 concentrations, averaging at 64 ppb (Figure 3a) and reaching > 70 ppb temporally (Figure 3b). Finally, Cluster 5 has, considerably, the lowest mid-level O_3 (Figure 3c) averaging at 45 ppb (Figure 3a), almost
310 10 ppb lower than the other clusters. Cluster 5 also has the most variable low-level O_3 diurnal pattern (Figure 3b) which could be attributed to the averaging of only five different profile curtains that were assigned to this cluster (Table 1).

Figure 4a illustrates the mean lidar O_3 2-D profile curtains for each of the clusters. For Cluster 1, 3, 4, and 5, higher O_3 concentrations in the low-level are captured during afternoon/evening time (12:00 – 21:00 EDT), with the highest low-level O_3 in Cluster 4 (> 70 ppb). This behavior follows the common diurnal pattern of O_3, that was distinguishable in Figure 3b. This
315 common O_3 growth reaches vertically to approximately 1500 m for each of the clusters but is generally contained below 2000 m. Differing from the low-level O_3 behavior, mid-level O_3 is generally less variable in magnitude throughout the entire profile curtain (except for Cluster 1; see Figure 3a). The highest O_3 concentrations for the mid-level are exhibited in Cluster 1, 2, 3, and 4, with the highest mid-level O_3 in Cluster 1 during the early morning hours (≥ 70 ppb).

Following the descriptions above, each cluster is given a nomenclature according to their unique characteristics. Cluster
320 1 is termed as the highest mid-level O_3 (HMO) cluster; Cluster 2 as the lowest low-level O_3 (LLO) cluster; Cluster 3 is the most common O_3 (MCO) cluster; Cluster 4 is the highest low-level O_3 (HLO); Cluster 5 is the least common and lowest mid-level O_3 (LMO) cluster. The O_3 variability represented and justified above is what led to the successful clustering of the lidar O_3 2-D profile curtains.

https://doi.org/10.5194/acp-2022-133
Preprint. Discussion started: 23 March 2022

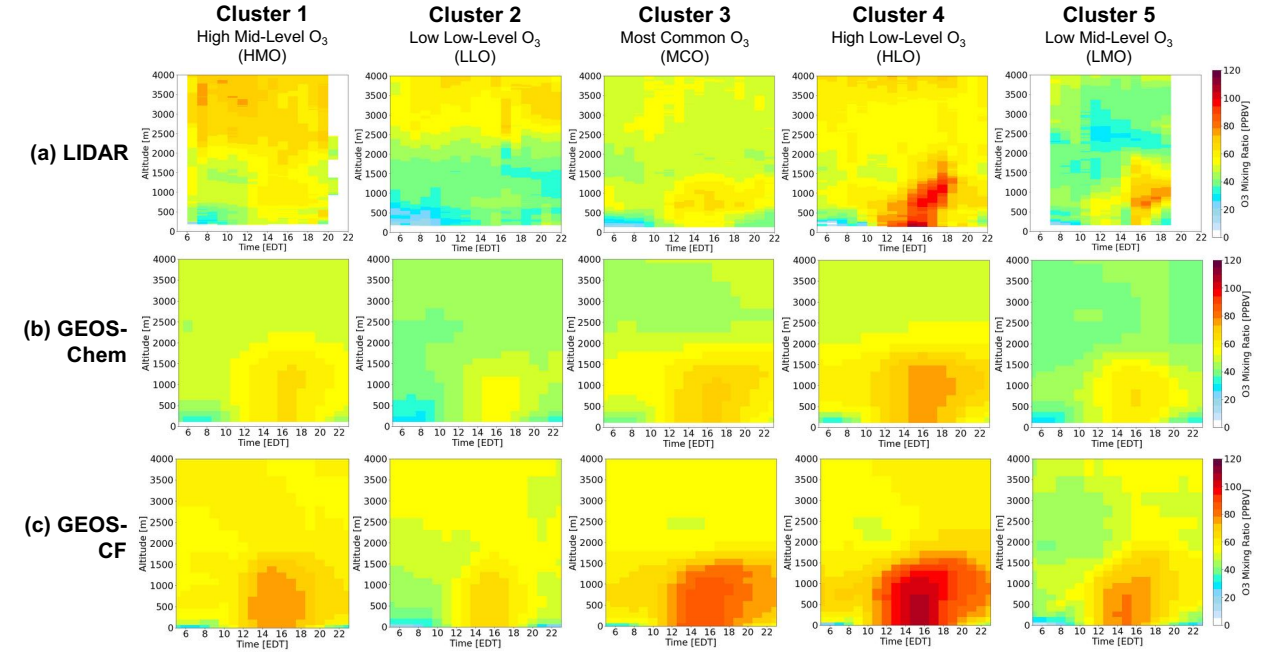

Figure 4. Cluster-mean O_3 vertical profile results by cluster assignment (1- 5) and arranged: a) LIDAR; b) GEOS-Chem simulation; and c) GEOS-CF simulation.

The clustering analysis results provided a characterization of O_3 behavior that transpired during these three campaigns. Figure 3c indicates each cluster represents a different photochemical regime and is useful in that it could demonstrate background O_3 in the case studies. HLO curtain profiles also had higher background O_3, indicating these cases did not have "clean air" to begin with which have allowed for a greater accumulation in the low-level. In another example, several curtain profiles assigned to the HMO cluster indicate concentrated residual layers in the mid-level and possible entrainment to the surface as the day progressed. To prove this feature, vertical velocity and vertical velocity variance data would be needed but the knowledge that a clustering approach is able to pinpoint these features proves to be useful. The clustering results was valuable in recognizing a significant large pollution related cluster (HLO), a total of 18 out of the 91 curtain profiles which correspond with the highest daily surface maxima measured at these sites (= 97.77 ppb) (Table 1). This cluster, on average, exhibited a daily surface maxima up to 10 ppb greater than any of the other clusters. Discerning these higher O_3 cases is imperative for mitigating severe air pollution.

3.2. Cluster meteorological surface analysis

To support the lidar clustering results, daily averaged meteorological surface observations from AQS stations pertaining to the campaign period and GEOS-Chem surface model output were evaluated in regard to the five clusters. Figure 5 shows the cluster mean surface temperature from AQS stations and GEOS-Chem model as well as the simulated wind speed and

https://doi.org/10.5194/acp-2022-133
Preprint. Discussion started: 23 March 2022

Atmospheric Chemistry and Physics Discussions

345 direction. The average surface temperature from each station is represented as the circular markers while the simulated temperatures are represented as the spatial contour and the simulated wind speed (m s^{-1}) and direction as arrows. Cluster average AQS surface temperature and wind speed can be found in Table 1d, e.

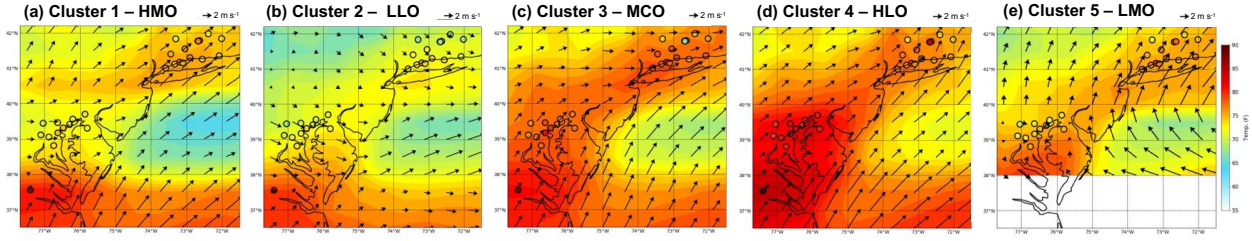

350 **Figure 5.** Meteorological surface observational and model simulated averages by cluster (a - e). Average surface temperatures from AQS stations are represented as the circular markers while simulated temperatures are represented as the spatial contour. Simulated winds are represented as the black arrows.

In general, the surface meteorological conditions agree with our knowledge of transport and O_3 production that would 355 lead to each of the five clustered lidar O_3 profile curtains. It is evident that the clusters with the highest surface O_3 (HMO, MCO, and HLO) all share a predominant offshore, westerly wind. Furthermore, MCO and HLO (Figure 5c, d) presented higher overall observed and simulated surface temperatures compared to the other clusters. Observed (not shown in Figure 5; see Table 1) and simulated wind speeds reveal slightly lower average wind speeds and primarily continental wind flow for both clusters as well. These meteorological conditions are conducive to a higher production of surface O_3 concentrations which 360 validates the higher O_3 found in the low-level results (Figure 3b, 4a).

Conversely, the lowest surface temperatures are found in LLO (Figure 5b). Lower surface temperatures are also indicative of low vertical mixing due to less generation of convection. Relatively calm wind speeds and lower temperatures indicate other possible meteorological factors such as high cloud cover that could have contributed to the lower O_3 concentrations in LLO. Although surface O_3 concentrations in LMO reach higher levels later in the day, first at 12:00 EDT and then again at 16:00 365 EDT, the rest of the temporal profile stays below moderate levels. In Figure 5e, average temperatures for LMO are moderately high but, in contrast, the average wind speed is higher (specifically over the Long Island Sound) and unique to the other clusters, wind direction is predominantly onshore (Easterly – Southerly). This prevalent onshore flow indicates a transport of cleaner marine air which corroborates the lower surface O_3 levels. LMO did not have any curtain profiles assigned from OWLETS-1 which is why data for the lower Chesapeake Bay area is not shown in Figure 5e.

370

3.3. Evaluating the GEOS-Chem and GEOS-CF model

In this sect. the model results from GEOS-Chem and GEOS-CF will be compared to the lidar data using the five lidar O_3 profile clusters discussed in Sect. 3.1. Both model results were sampled in an equal manner, in which we extracted the same

https://doi.org/10.5194/acp-2022-133
Preprint. Discussion started: 23 March 2022

Atmospheric Chemistry and Physics Discussions

cluster date assignments from the lidar clusters and created mean vertical profiles based on the model results. This allowed us to evaluate the model performance based on the five characterized O_3 lidar clusters. As mentioned previously, the GEOS-CF simulation data is not available for 2017. Thus, the results shown subsequently will only include GEOS-CF results from 2018 (only dates from the OWLETS-2 and LISTOS campaigns). The GEOS-Chem simulation results include both years thus all three campaign duration periods.

3.3.1 Overall model performance

In Figure 6, we first evaluate the overall relationship and correlation between both models and the lidar data, disregarding the specific clusters. The comparisons are separated by the two different altitude subsets as the performances are strikingly different between low-level and mid-level for both GEOS-Chem (Figure 6a) and GEOS-CF (Figure 6b). In general, the models perform better simulating O_3 behavior in the low-level than the mid-level for all five clusters.

The overall correlation indicates that GEOS-CF (R = 0.69) has a slightly stronger correlation than GEOS-Chem (R = 0.66) in the low-level (Figure 6 - top panel). For both models, correlation is higher than 0.51, signifying a fair relationship between the model simulations and the lidar observations. The overall correlation reveals that GEOS-CF is marginally superior to GEOS-Chem in the mid-level but both models have a fairly weak relationship at this altitude range (R = 0.22 and R = 0.12, respectively) (Figure 6 - bottom panel). The overall correlation analysis provides a fundamental but condensed assessment of model performance. In the next sect., the cluster specific differences reveal additional model performance insight that would be conceivably overlooked when evaluating overall performance.

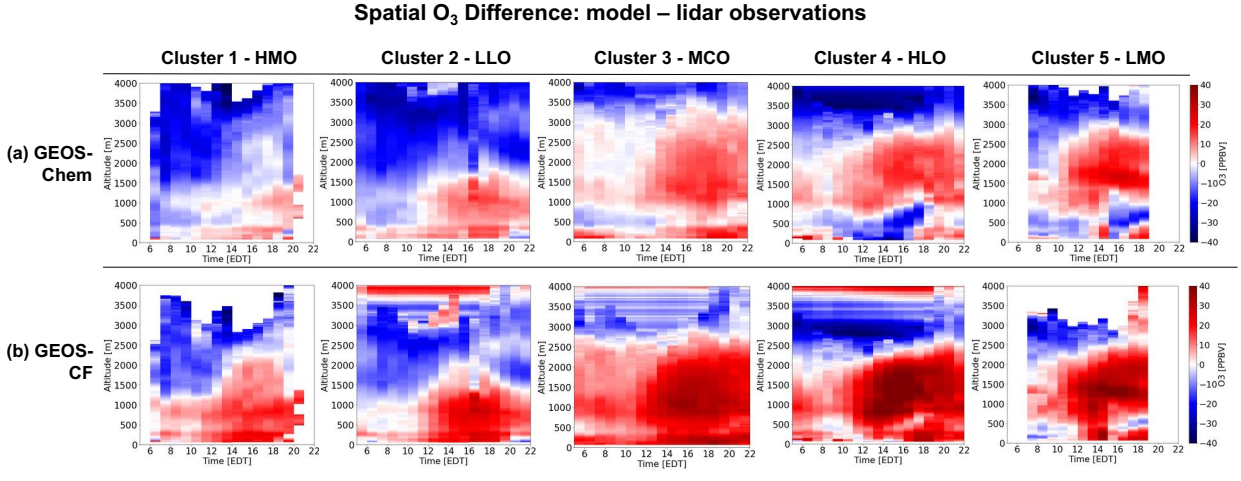

Figure 6. Spatial O_3 difference (model – lidar observations) for each cluster (1 – 5). GEOS-Chem differences (a) and GEOS-CF difference (b).

3.3.2 Model evaluation based on lidar clusters

https://doi.org/10.5194/acp-2022-133
Preprint. Discussion started: 23 March 2022

Atmospheric Chemistry and Physics Discussions

In evaluating the models based on the established O_3 behavior cases, significant cluster by cluster differences are unmasked. Figure 4b and 4c depict the simulated cluster-mean O_3 profile curtains from GEOS-Chem and GEOS-CF, mirroring the mean lidar curtains in Figure 4a. For all clusters in the low-level, both models simulate a continuous accumulation of O_3 near the surface after 12:00 EDT, mirroring the O_3 common diurnal pattern depicted in mean lidar curtains in Figure 4a. However, the extent the models simulate is often higher in magnitude than the observations, specifically GEOS-CF predicting the accumulation at a higher magnitude than GEOS-Chem. In the mid-level, both models simulate much less O_3 variability than what is captured in the lidar observations. Figure 4b and 4c clearly show how the models struggle to reproduce the intricate O_3 pattern and variability that is relayed in the lidar observations (Figure 4a), especially in the mid-level. To compare and quantify the results illustrated in Figure 4, modeled versus lidar observation spatial O_3 differences were derived for each cluster (Figure 7). Figure 7 highlights the explicit spatiotemporal model differences compared to the lidar curtains for each cluster. The cluster specific percent biases and correlation statistics, found in Table S1 and Figure S4 (in Supplementary Material), were calculated from the total vertical and diurnal averages separated by low-level and mid-level.

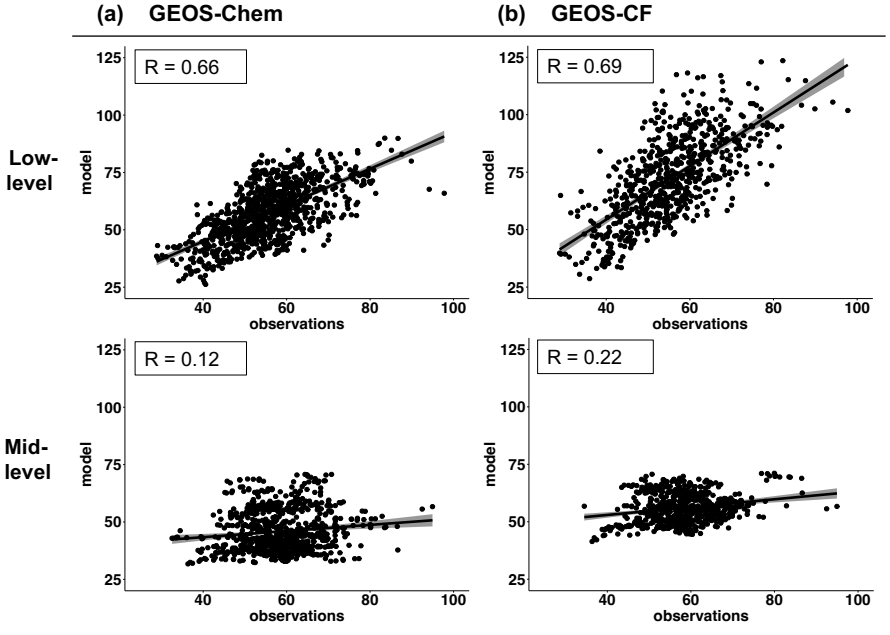

Figure 7. Overall O_3 correlation between the lidar observations versus a) GEOS-Chem and b) GEOS-CF split by low-level (top panel) and mid-level (bottom panel).

GEOS-Chem performs well in simulating low-level O_3 with a lower non-systematic percent bias ranging from -0.051 to +0.068 % for the five clusters. GEOS-Chem has a slightly lower correlation than GEOS-CF in the low-level (R = 0.51 – 0.61) but still indicates a reasonable relationship with the lidar observations. GEOS-Chem also has a non-systematic bias in the low-level. Thus, GEOS-Chem can simulate the variability of O_3 and based on the lower bias, the magnitude as well. In all five

https://doi.org/10.5194/acp-2022-133
Preprint. Discussion started: 23 March 2022


Atmospheric Chemistry and Physics Discussions

clusters, GEOS-CF overestimates the average magnitude of low-level O_3 with a systematic high positive percent bias ranging from +0.139 to +0.340 % (Table S1). GEOS-CF has a relatively good correlation (R = 0.54 - 0.74) but a consistently high bias compared to the lidar observations (Table S1 and Figure S4, Supplementary Materials). From the estimated differences (Figure 7), this can be attributed predominantly to GEOS-CF overestimating afternoon O_3.

In the low-level, GEOS-Chem has the best performance (minimal +0.020 % bias) in LLO, which is the cluster with the lowest O_3 accumulation. The second-best performance for GEOS-Chem in the low-level follows closely behind (minimal -0.026 % bias) in HLO, the cluster with the highest O_3 accumulation. These results suggest GEOS-Chem performs well in the low-level but has a tendency to overpredict lower O_3 concentrations and underpredict higher O_3 concentrations. GEOS-CF has a similar performance in the low-level for HMO, LLO, and LMO with positive percent biases at 0.139, 0.189, and 0.197 %, respectively. This implies GEOS-CF has a better ability capturing lower O_3 concentrations below 2000 m than higher concentrations, such as MCO and 4. Both models have the worst performance in MCO with a +0.068 % bias for GEOS-Chem and +0.340 % bias for GEOS-CF. As described in Sect. 3.1, MCO is the most common cluster with moderately high average O_3 concentrations (refer to Figure 3b). As both models have the highest bias for this cluster, this suggests neither model is fully able to simulate moderately high O_3 in the low-level which was a frequently occurring event for this study period.

In the mid-level, GEOS-Chem performs poorly, consistently underestimating O_3 to a significant magnitude. In all five clusters, GEOS-Chem underestimates the magnitude of mid-level O_3 with a systematic high negative percent bias ranging from -0.268 to -0.096 % (Table S1). GEOS-Chem also has a low correlation in the mid-level (R = -0.26 – 0.23). Thus, GEOS-Chem is not able to simulate the variability of O_3 nor the magnitude well in the mid-level. GEOS-CF performs slightly better than GEOS-Chem in simulating mid-level O_3 with a lower and non-systematic percent bias for the five clusters ranging from -0.143 to +0.112 %. GEOS-CF has a marginally stronger correlation to the lidar observations than GEOS-Chem for all clusters except MCO, where GEOS-Chem has -0.26 correlation and GEOS-CF has a -0.19 correlation (Figure S4, Supplementary Materials). Thus, GEOS-CF, in some cases, is better able to simulate the O_3 variability in the mid-level (R = -0.19 – 0.74) and based on the lower bias, the magnitude as well.

Both models underestimate mid-level O_3 magnitude to the greatest extent in HMO, which is the cluster with the highest mid-level O_3 concentrations (refer to Figure 3c). This implies that the models struggle to simulate higher concentrations of O_3 in the mid-level ($\geq$ 70 ppb). GEOS-CF does best simulating LLO, MCO, and HLO, all clusters with moderate mid-level O_3 averages ($\leq$ 60 ppb). On the other hand, the GEOS-Chem model never reaches O_3 cluster averages greater than 50 ppb, which directly divulges the greater systemic negative bias in the mid-level. GEOS-Chem simulates LMO mid-level O_3 the best (-0.096 percent bias), which is the cluster with the lowest O_3 average (< 45 ppb) indicating GEOS-Chem is relatively capable of simulating mid-level O_3 only when the case devises lower concentrations.

3.3.3 Cluster approach and model conclusions

Evaluating the clustered O_3 lidar profile curtains against CTMs allowed us to conclude that for cases of high O_3 in the low-level, GEOS-Chem was able to simulate but underestimates the extent of high O_3 near the surface while GEOS-CF

https://doi.org/10.5194/acp-2022-133
Preprint. Discussion started: 23 March 2022


Atmospheric Chemistry and Physics Discussions

struggled to simulate and overestimates these high O_3 cases. Previous studies have found that excessive vertical mixing has led to overestimation of O_3 near the surface as well as underestimation of O_3 night-time depletion led to overestimation of O_3 the next day (Dacic et al., 2020; Keller et al., 2021; Travis & Jacob, 2019). The titration that occurs at night after the initial afternoon build up requires successful simulation to prevent the model beginning the following day with higher O_3 than is observed which can lead to the overprediction of O_3 later that day. Therefore, in the given case there is an O_3 event that lasts more than one day (at the same lidar location), the model will likely underestimate O_3 night-time depletion, overpredict morning O_3, and subsequently overpredict the afternoon build-up. Being as there were multiple cases (17 total from HMO, MCO, and HLO) of multi-day high O_3 events, this is likely one of the main reasons for GEOS-CF overestimating afternoon O_3 in these high low-level O_3 cases. In Figure 7, GEOS-CF exhibits the greatest midday O_3 overprediction in MCO and HLO. In HLO alone, there were 4 (out of 18) of the profiles that were consecutive while in MCO there were 8 (out of 28). This gives explanation for upwards of 22 – 29 % of the overestimation of O_3 in the profile curtains of these clusters. These multi-day O_3 events are particularly important as they can indubitably lead GEOS-CF to higher overprediction of afternoon O_3.

Contrarily, GEOS-Chem underpredicts O_3 in the morning times which does not allow for the same build-up up of midday O_3 distinct in the lidar curtain profiles. This could explain why GEOS-Chem underpredicts the clusters with higher O_3 concentrations in the low-level. Additionally, the low and non-systemic bias in the low-level for GEOS-Chem demonstrates that the model does not have such an issue simulating the correct magnitude of O_3 but instead, the lower correlations suggest that GEOS-Chem merely struggles to simulate the pattern. This is most apparent in the MCO cluster where GEOS-Chem predicts a spatially larger build-up of O_3 but essentially does well in simulating the correct magnitude. This model gap can then be attributed to the coarser model resolution not being able to reproduce finer O_3 pattern behavior such as is evident in the lidar curtain profiles.

In the mid-level GEOS-Chem has a systemic high negative bias for all clusters except the LMO cluster. It is evident that the model cannot simulate cases with higher O_3 concentrations in the mid-level. On the other hand, GEOS-CF performs better with a lower non-systemic bias in the mid-level. Since GEOS-Chem was run with the tropchem chemistry mechanism which excludes stratospheric chemistry and GEOS-CF uses the UCX chemistry mechanism that includes stratospheric chemistry, this may allude to better performance of GEOS-CF in simulating higher O_3 concentrations in the mid-level. Both models indicate weak correlations with the lidar observations in the mid-level and it is apparent that both models struggle to capture the pattern of O_3 behavior in the mid-level. This is likely due to the model resolutions. Although GEOS-CF has a finer resolution than GEOS-Chem, it still may not be sufficient in horizontal and vertical grid resolution to replicate the finer O_3 variations captured in the 2-D lidar observations.

Although this analysis proves to be a useful technique to characterize O_3 behavior over a period of time and to evaluate the ability of model to simulate the largely variably O_3 behavior, there are also limitations. In this study we are comparing single point lidar versus model output, therefore we cannot simply state that the model is incorrect. We make conclusions and draw biases based on the ability to subset a grid point and compare that to a single point lidar curtain to the best ability but there is still uncertainty. Ozone lidars have a unique advantage, compared to traditional surface measurements, in measuring

https://doi.org/10.5194/acp-2022-133
Preprint. Discussion started: 23 March 2022


Atmospheric Chemistry and Physics Discussions

vertical distribution of O_3 with respect to time. The high vertical and spatiotemporal resolution reveal intricate details about the behavior of O_3 during these campaigns. Lidars still have limitations that prove to be a complication e.g., noise signal and manual operations. At the time of writing, the operative limitation has been addressed and the lidars are now more fully automatized which removes some of the difficulty.

Several studies rely on case study investigations to evaluate model performance in coastal regions. Another approach, demonstrated in Sect. 3.3.1, would be to simply group data by altitude to achieve a summarized model evaluation. However, a systematic and comprehensive understanding of the different photochemical regimes in coastal regions does not only require case studies and overall summaries. The clustering approach allows for a comprehensive yet still detailed evaluation of the different photochemical regimes in coastal regions and the model performances in these cases. Looking at the overall correlations (Figure 6), both models seem to have a good relationship with the low-level lidar observations. But, in applying a clustering method we can analyze cluster-by-cluster differences (Figure 7) and the gaps within the models are elucidated. Using the clustering, we are able evaluate how the cluster specific differences reveal additional model performance insight that would be conceivably overlooked when evaluating overall performance.

3.4 Impact of meteorological factors on clusters & model performance

Meteorological factors such as wind speed and direction can directly impact whether a coastal region will experience clean air or O_3 exceedances. When local meteorological processes such as sea/bay breeze occur at such a fine scale, equally fine resolution measurements are essential in capturing this. To evaluate the relationship between lower tropospheric temporal and vertical wind structure and O_3 and assess model performance, Doppler wind lidar and modeled wind profiles are analyzed in accordance with the O_3 lidar profiles under the five different clusters. The Doppler wind lidar data is unique in that it offers a focus on fine details that are only revealed in the multi-dimensional data which allows for such a comprehensive evaluation of the established O_3 cluster profiles.

3.4.1 Doppler wind lidar and simulated wind case studies

In this sect., hourly averaged GEOS-Chem and GEOS-CF modeled wind vertical and temporal profiles were compared to Doppler wind lidar 2-D profiles observed during the OWLETS-2 campaign at HMI. In comparing the two models with the observations, the online meteorological capabilities of GEOS-CF will be evaluated along with the offline GEOS-Chem efforts. The wind lidar ran for a total of 23 days during OWLETS-2 but for this model comparison, five 2-D profile curtains, one belonging to each cluster, were chosen as case studies to represent the five different clusters. HMO is represented by 29 June 2018, LLO: 24 June 2018, MCO: 17 June 2018, HLO: 30 June 2018, and LMO: 20 June 2018. The same dates were used for the modeled profiles. In Figure 8, the Doppler wind lidar profile curtains are compared with GEOS-Chem and GEOS-CF simulated profile curtains for the five case studies. There are consistent Doppler lidar measurements throughout the low-level (< 2000 m) which allows for a direct comparison with the simulated profiles; therefore, the focus of the following analysis will be on the low-level altitudes.

https://doi.org/10.5194/acp-2022-133
Preprint. Discussion started: 23 March 2022

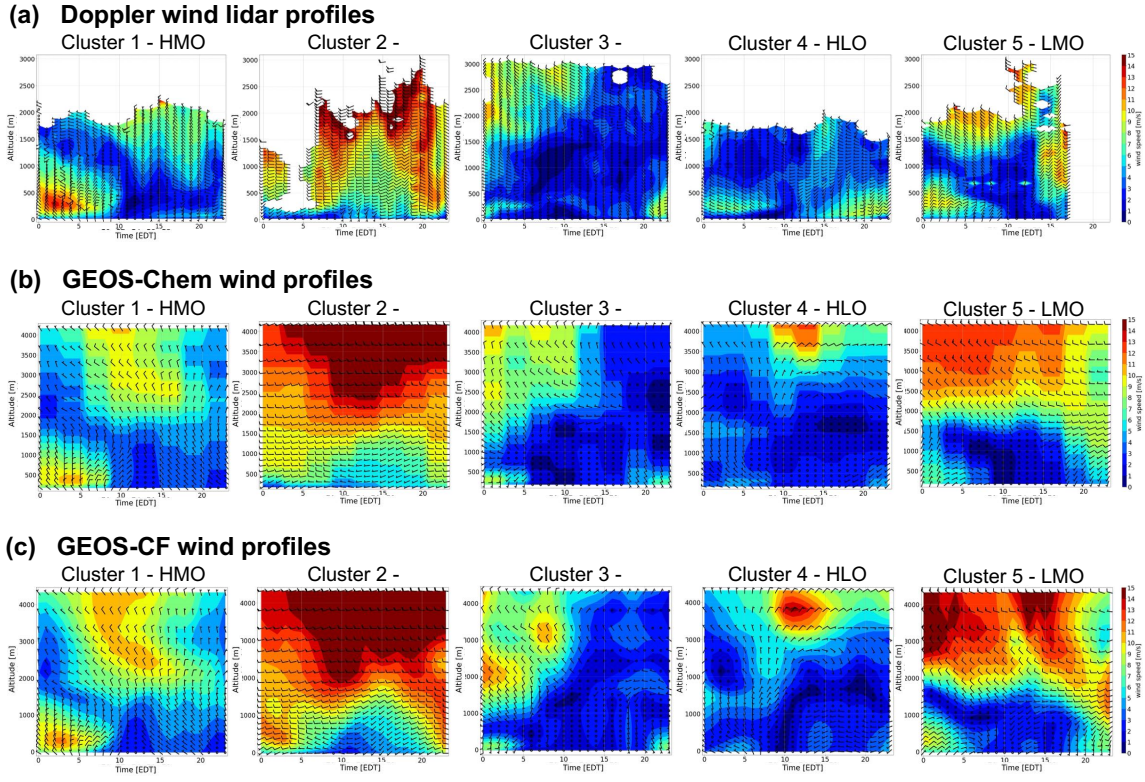

Figure 8. Vertical profiles of wind speed and direction from a) Doppler wind lidar, b) GEOS-Chem, and c) GEOS-CF model results from OWLETS-2 at HMI. Each figure depicts a date assigned to a specific cluster (1 - 5).

For the HMO case study, both models did generally well simulate the observed wind speeds but slightly struggle with the timing. There is an observed increase in wind speed near the surface beginning at 1:00 EDT (Figure 8a), but both models predict this peak of this increase a bit later (at about 3:00 EDT). Observed wind speeds remain generally higher for a longer period of time to 10:00 EDT, while only simulated to about 8:00 EDT. Both models underestimate the high wind speeds at this time, with GEOS-Chem underestimating about 4 m s^{-1} and GEOS-CF about 3 m s^{-1}. Along with the wind maxima in the morning, there is a wind direction change observed later in the profile, beginning at about 10:00 EDT. Both models are able to simulate the timing of this change fairly but not the actual wind direction. The LLO case study observed high winds throughout the majority of the vertical and temporal profile, with calmer winds just directly above the surface (< 500 m). The models slightly underpredict low-level wind speeds in LLO. The models struggle to capture the minor wind direction shift from offshore (N – W) to onshore (E – S) directly at the surface at 10:00 – 14:00 EDT, although winds just above 500 m remained offshore throughout the vertical and temporal profile. The finer resolution of GEOS-CF seems to help in simulating the pattern of wind speed but not the magnitude. This is most apparent in LLO where the distinct vertical wind speed pattern

https://doi.org/10.5194/acp-2022-133
Preprint. Discussion started: 23 March 2022


Atmospheric Chemistry and Physics Discussions

in the lidar curtain is replicated better by GEOS-CF than GEOS-Chem. Although, the resolution still does not seem to be fine enough to resolve the intricate vertical wind speed and direction patterns.

GEOS-Chem and GEOS-CF both struggle to capture low-level wind speed and direction in MCO, HLO, and LMO with the poorest performances in MCO and HLO. In MCO, the Doppler wind lidar captures a wind direction shift from westerly to easterly winds beginning at 6:00 EDT accompanied by calm winds (approximately 0 m s^{-1}) indicating a likely common sea/bay breeze event. The timing of the start of this event is simulated well but the models fail to predict an actual well-defined wind shift, instead merely simulating 0 m s^{-1} winds after 5:00 EDT. It is apparent that the models struggle to capture the finer processes such as a sea/bay breeze which could have likely led the underprediction of wind speed. A wind direction shift is also depicted in HLO, with westerly winds early in the morning and a shift to south-easterly winds later in the temporal profile (at about 10:00 EDT). This could also likely be an early onset sea breeze event which could have contributed to the high observed O_3 concentrations in the afternoon. Again, the exact timing of the start of the wind shift is captured by the models but then no defined shift and little to no winds are simulated after. There are two cases of observed increased wind speeds near the surface, first at 0:00 – 8:00 EDT then again at 14:00 – 24:00 EDT. Both models underestimate the extent of the increased wind speeds. LMO does not have the same wind direction shift but instead has a more consistent easterly flow near the surface and an offshore flow aloft which is simulated well with a slight underprediction of winds earlier in the morning. Since the Doppler lidar measurements lack consistent data above 2000 m, it is unfeasible to evaluate and make definite conclusions on the modeled mid-level winds. Therefore, we ultimately cannot accurately validate the high biases and underprediction of mid-level O_3 (Figure 4, Table S1), specifically for GEOS-Chem, in relation to the modeled winds. This suggests the need for more multi-dimensional wind profiling and other measurements in future field campaigns.

3.4.2 Ozone and winds in relation to lidar measurements

In this sect., the Doppler wind lidar 2-D curtains will be assessed relative to the O_3 lidar clusters and the model performance. These cases represent possible wind and O_3 situations in the clusters therefore they cannot explicitly explain cluster biases and results. In LLO a slight underprediction of wind speed below 1000 m may have led to the slight overprediction of O_3 for both models, especially for GEOS-CF. While the average low-level O_3 bias for LLO was relatively low, the model vertical profile captured a build-up of O_3 at 12:00 EDT that was not captured by the lidar (Figure 4a).

For the observed and simulated winds in HMO, a possible entrainment of elevated O_3 into the PBL as the surface mixing layer grows from morning to midday (at 12:00 EDT) would be possible, in the case that the elevated O_3 layer is low enough (Figure 4a). Further analysis such as vertical velocity and vertical velocity variance data would be needed to corroborate this. The wind maxima captured at 5:00 EDT also could indicate evidence of a low-level jet near the surface following a stationary cold front. In the case of a low-level jet, high wind speeds can act to transport clean air masses that would likely lead to lower O_3 concentrations later in the afternoon. This is apparent in Figure 4a in which, near the surface, early morning lower O_3 concentrations (< 40 ppb) inhibited a greater accumulation of afternoon O_3 build-up. The early wind maxima in HMO near the surface was underpredicted by both models. An underprediction of wind maxima early in the morning could have led to a case

https://doi.org/10.5194/acp-2022-133
Preprint. Discussion started: 23 March 2022


Atmospheric Chemistry and Physics Discussions

of overprediction of O_3 later in the afternoon. This is most apparent in GEOS-CF which overpredicts low-level O_3 throughout the temporal profile in HMO. The convergence zone apparent in HMO at about 10:00 EDT is also indicative of a possible sea/bay breeze occurrence. The inability of the models to simulate the correct wind direction can lead to an inability to correctly simulate low-level O_3. GEOS-Chem has its second worst performance simulating low-level O_3 in HMO (high percent bias and lower correlation) which is likely contributed by this convergence in low-level winds.

Sect. 3 revealed that both models had the highest bias and lowest correlation simulating low-level O_3 in MCO. GEOS-CF also poorly simulated low-level O_3 in HLO with the second highest percent bias. Evaluating the wind lidar profile against the simulated winds helps paint a better picture as to why. As mentioned in Sect. 3.4.1, both MCO and HLO depict wind shifts throughout the temporal profile that likely indicate the development of a sea/bay breeze. In most cases, sea/bay breeze events can contribute to high concentrated daytime O_3 events in which O_3 is recirculated throughout the region. Such cases would likely lead to a similar curtain profile as seen for HLO. But the cases for MCO and HLO are dissimilar. Both models overpredict low-level O_3 in MCO but only GEOS-CF overpredicts low-level O_3 in HLO. GEOS-Chem actually underestimates low-level O_3 in HLO. For MCO, the overestimation of low-level O_3 can be delineated by the underestimated wind speeds throughout the majority of the temporal profile. What is peculiar is that for HLO, GEOS-CF performs well simulating the timing and wind shift than GEOS-Chem. It is important to denote that although GEOS-CF has a much greater percent bias for low-level O_3 in HLO, the model had a reasonable relationship ($R = 0.61$) with the O_3 lidar measurements. This is corroborated with the ability of GEOS-CF to better simulate wind pattern shifts in HLO. While GEOS-Chem has a lower percent bias for low-level O_3 in HLO, GEOS-Chem consistently underestimates wind speed and fails to reproduce any wind shifts.

The cases divulged for MCO and HLO give even more reason to address the difficulty simulating complex coastal mechanisms. Despite the fact that MCO and HLO both indicated prospective sea/bay breeze cases, the results of the simulated winds and O_3 were distinctive. Simulating complex sea/bay and land relations is imperative for correctly mitigating high O_3 cases. To accurately simulate such complex exchanges, high resolution vertical and horizontal simulations are needed. Because of the models' relatively coarse resolutions (nominally 50 and 25 km horizonal resolution; 72 vertical levels), the fine-scale vertical wind gradients and horizontal wind shifts are difficult to resolve and, in these cases, not fully able to replicate.

LMO presents a unique wind case in which there is an early morning north-easterly flow that was well replicated by the models. Since both models had moderately high percent biases and lower correlations for LMO, this implies that winds are not the sole factor contributing to a misrepresentation of modeled O_3 concentrations. This study acknowledges the need for an evaluation of other modeled factors, such as precursor emissions or fire smoke transport, considering the possible confounding effects on modeled O_3 outcome.

4. Conclusion

We developed and tested a clustering method on a suite of 91 multi-dimensional lidar O_3 profile curtains retrieved from three recent land/sea campaigns (OWLETS 1, OWLETS 2, and LISTOS), during the summer months of 2017 and 2018. The K-Means clustering algorithm, driven by 8 well defined features, was applied to categorize the fine resolution O_3 data,

https://doi.org/10.5194/acp-2022-133
Preprint. Discussion started: 23 March 2022


Atmospheric Chemistry and Physics Discussions

revealing five distinct O_3 behavior cases that are unique in pattern and magnitude vertically and temporally. We present five different cases of O_3 behavior identified as: highest mid-level O_3 (HMO) cluster; lowest low-level O_3 (LLO) cluster; most common O_3 (MCO) cluster; highest low-level O_3 (HLO); lowest mid-level O_3 (LMO) cluster. The results indicate that fine resolution data can be used to differentiate the behavior of O_3 in a region and classify different cases of O_3 exploiting the multiple dimensions. The clustering approach allowed us to characterize the range of highly variable vertical and temporal coastal O_3 behavior for the duration of these campaigns which can be a good indicator of how O_3 behaves in general in these coastal regions during the summer months. Furthermore, this approach could be used by states to better identify different O_3 photochemical regimes and frequency beyond just surface sampling.

The clustering analysis provided an abridged method to evaluate the performance of two CTMs, GEOS-Chem and GEOS-CF, in these complex environments. The curated cluster results concluded in this study reveal current limitations and also cases in which the CTMs fare well in simulating coastal O_3. It is concluded that GEOS-Chem simulates low O_3 concentrations best in the low-level altitude (e.g., in LLO), while both models struggled to capture moderately high O_3 behaviors in the low-level altitudes (e.g., in MCO). GEOS-Chem had overall low unsystematic bias range and fair relationship with the lidar observations ($R = 0.66$) in the low-level. GEOS-CF had a systematic high positive bias but overall fair relationship ($R = 0.69$) in the low-level. It is concluded that both models were able to simulate low-level O_3 pattern well, but GEOS-CF was not able to simulate the magnitude consistently overestimating O_3 in the low-level altitude.

Overall, the models have the greatest difficulty simulating the vertical extent and variability of O_3 concentrations in the mid-level. Both models underestimate mid-level O_3 with the worst performance in HMO, while lower O_3 concentrations are better simulated by both models in mid-level altitudes. In the mid-level, GEOS-Chem and GEOS-CF both have a weak relationship with the lidar observations ($R = 0.12$ and 0.22, respectively). GEOS-Chem had a systematic high negative bias and GEOS-CF an overall lower unsystematic bias range. Thus, neither model simulated the mid-level O_3 pattern well, but GEOS-CF was able to simulate the magnitude slightly better than GEOS-Chem. Since the GEOS-CF model is run with the combined tropospheric and stratospheric chemistry mechanism (UCX chemistry mechanism), we can expect the performance of this model in the mid-level to be superior to the GEOS-Chem tropchem mechanism which only considers tropospheric chemistry. Although the overall correlation results indicate GEOS-CF, which has a better grid resolution and is an online model, had a slightly better relationship with the lidar observations than GEOS-Chem, it can be concluded that there are still limitations to both models especially when simulating mid-level O_3. Known model errors and coarse horizontal and vertical grid resolution contribute to the difficulty in simulating fine-scale coastal O_3 variability.

Modeled winds were evaluated using Doppler wind lidar data observed during the OWLETS-2 campaign. The wind lidar data was mostly limited to lower altitudes (< 2000 m), which allowed for wind speed and direction validation at the low-level. The deficit of mid-level observed wind data disallows for a conclusive and concrete evaluation of simulated mid-level O_3. In the low-level, there was a general underprediction for the selected case studies evaluated for all 5 clusters with the poorest modeled results found in MCO and HLO. The morning wind deceleration and directional shifts (onshore to offshore) illustrated in the lidar profiles indicated a possible sea/bay breeze event in both clusters. This likely led to cases of enhanced

https://doi.org/10.5194/acp-2022-133
Preprint. Discussion started: 23 March 2022


Atmospheric Chemistry and Physics Discussions

surface O_3 in these clusters. Due to the coarser model resolution, GEOS-Chem and GEOS-CF were not able to capture the sea breeze phenomena in these cases which could have facilitated in the high O_3 biases for these clusters. With GEOS-CF having a finer horizontal resolution than GEOS-Chem, the results reveal advantages for GEOS-CF simulating the pattern of wind speeds better. But the finer resolution did not help in simulating wind directional shift as in MCO and HLO. This affirms that the spatial resolution of GEOS-CF (~25 km) is still not fine enough for mesoscale processes such as the sea/bay breeze. Ultimately, the vertical resolution for both models was too coarse to resolve fine-scale vertical wind gradients. We acknowledge that an evaluation of other factors, such as model precursor emissions or chemical mechanisms, is needed to fully evaluate the discrepancies in modeled coastal O_3.

This work is the first time that all three associated campaign lidar data have been analyzed in conjunction. In utilizing the highly detailed suite of multi-dimensional lidar data, we are able to explore the behavior and variability of coastal O_3 for the duration of the campaigns. Applying the clustering analysis directly to the lidar O_3 data emerges as a useful and robust approach for identifying O_3 patterns during the highly polluted summer months in coastal environments. Since the time of the OWLETS and LISTOS campaigns, the lidar instrument systems have been updated and are now more fully automatized for use eliminating such constraints faced in this study. Further observations using lidar instruments should be especially valuable in investigating coastal O_3 behavior as it can divulge the finer-scale O_3 characteristics that remain difficult to successfully simulate in CTMs. The time-height and fine resolution measurements only available from multi-dimensional lidar instruments were vital in allowing us to form these conclusions.

This kind of evaluation allows for detailed model assessment of specific O_3 cases that are unmasked through the clustering analysis. Looking at the overall correlations, it would seem the models have a good relationship with the low-level lidar observations but looking into the cluster-by-cluster differences, the gaps within the models are elucidated. Using the cluster assignments, we are able evaluate how the cluster specific differences reveal additional model performance insight that could be conceivably overlooked when evaluating overall performance. This work is a middle ground between looking at specific cases (or dates) and summarizing overall model performance. We provide a new approach that allows a synopsis of summer coastal O_3 behavior and subsequently model performance without completely muting distinct O_3 features. Evaluating model performance for diverse O_3 behavior in coastal regions is crucial for improving the simulation and furthermore, mitigation of air quality events.

Code availability. Model code is available upon request to the first author.

Data availability.

Supplement.

Author contributions. CB and YW conceived the research idea. CB wrote the initial draft of the paper and performed the analyses and model development. All authors contributed to the interpretation of the results and the preparation of the paper.

https://doi.org/10.5194/acp-2022-133
Preprint. Discussion started: 23 March 2022

Competing interests. The authors declare that they have no conflict of interest.

Acknowledgements. This study is supported by NASA MUREP Graduate Fellowship (80NSSC19K1680). The Ozone Water-Land Environmental Transition Study (OWLETS-1, 2) and Long Island Sound Tropospheric Ozone Study (LISTOS) field measurements described here were funded by the NASA's Tropospheric Composition Program and Science Innovation Fund (SIF), Maryland Department of Environment, the National Oceanic and Atmospheric Administration (NOAA), the Environmental Protection Agency (EPA), the Northeast States for Coordinated Air Use Management (NESCAUM), and the New Jersey and Connecticut Departments of Energy and Environmental Protection. The authors acknowledge the principal investigators and data operators John Sullivan, Joel Dreessen, Ruben Delgado, William Carrion, and Joseph Sparrow as well as the guidance of the Tropospheric Ozone Lidar Network (TOLNet). LMOL and TROPOZ data are publicly available at (https://www-air.larc.nasa.gov/missions/TOLNet/). The OWLETS and LISTOS data are available at (https://www-air.larc.nasa.gov/). The Doppler wind data taken from the UMBC wind lidar and are publicly available at (https://www-air.larc.nasa.gov/cgi-bin/ArcView/owlets.2018). The GEOS-CF model simulation data were provided directly from the NASA Center Global Modeling and Assimilation Office (GMAO) at the Goddard Space Flight Center (https://gmao.gsfc.nasa.gov/weather_prediction/GEOS-CF/).

References

A., Little Roderick J, and Donald B. Rubin. Statistical Analysis with Missing Data. Second ed., Wiley, 1987.

Alonso, A.M., et al. "Time Series Clustering Based on Forecast Densities." Computational Statistics & Data Analysis, vol. 51, no. 2, 2006, pp. 762–776., https://doi.org/10.1016/j.csda.2006.04.035.

Banta, R. M., Senff, C. J., Nielsen-Gammon, J., Darby, L. S., Ryerson, T. B., Alvarez, R. J., Sandberg, S. P., Williams, E. J., & Trainer, M. (2005). A bad air day in Houston. Bulletin of the American Meteorological Society, 86(5), 657–670. https://doi.org/10.1175/BAMS-86-5-657

Bernier, Claudia, et al. "Clustering Surface Ozone Diurnal Cycles to Understand the Impact of Circulation Patterns in Houston, TX." Journal of Geophysical Research: Atmospheres, vol. 124, no. 23, 2019, pp. 13457–13474., https://doi.org/10.1029/2019jd031725.

Caicedo, Vanessa., et al. "Bay Breeze and Sea Breeze Circulation Impacts on the Planetary Boundary Layer and Air Quality from an Observed and Modeled Discover-AQ Texas Case Study." Journal of Geophysical Research: Atmospheres, 2019, https://doi.org/10.1029/2019jd030523.

Charrad, Malika, et al. "NBCLUST: An R package for Determining the Relevant Number of Clusters in a Data Set." Journal of Statistical Software, vol. 61, no. 6, 2014, https://doi.org/10.18637/jss.v061.i06.

Christiansen, Bo. "Atmospheric Circulation Regimes: Can Cluster Analysis Provide the Number?" Journal of Climate, vol. 20, no. 10, 2007, pp. 2229–2250., https://doi.org/10.1175/jcli4107.1.

Coggon, Matthew M; Gkatzelis, Georgios I; McDonald, Brian C; Gilman, Jessica B; Schwantes, Rebecca H; Abuhassan, Nader; Aikin, Kenneth C; Arend, Mark F; Berkoff, Timothy A; Brown, Steven S; "Volatile chemical product emissions enhance ozone and modulate urban chemistry", Proceedings of the National Academy of Sciences, 118,32,2021, National Academy of Sciences

Couillard, Maxim H; Schwab, Margaret J; Schwab, James J; Lu, Cheng-Hsuan; Joseph, Everette; Stutsrim, Brennan; Shrestha, Bhupal; Zhang, Jie; Knepp, Travis N; Gronoff, Guillaume P; "Vertical Profiles of Ozone Concentrations in the Lower Troposphere Downwind of New York City during LISTOS 2018-2019", Journal of Geophysical Research: Atmospheres, e2021JD035108,2021,

Darby, Lisa S. "Cluster Analysis of Surface Winds in Houston, Texas, and the Impact of Wind Patterns on Ozone." Journal of Applied Meteorology, vol. 44, no. 12, 2005, pp. 1788–1806., https://doi.org/10.1175/jam2320.1.

Davis, Robert E., et al. "A Comparison of Trajectory and Air Mass Approaches to Examine Ozone Variability." Atmospheric Environment, vol. 44, no. 1, 2010, pp. 64–74., https://doi.org/10.1016/j.atmosenv.2009.09.038.

De Young, Russell, et al. "Langley Mobile Ozone LIDAR: Ozone and Aerosol Atmospheric Profiling for Air Quality Research." Applied Optics, vol. 56, no. 3, 2017, p. 721., https://doi.org/10.1364/ao.56.000721.

Dreessen, Joel, et al. "Observed Ozone over the Chesapeake Bay Land-Water Interface: The Hart-Miller Island Pilot Project." Journal of the Air & Waste Management Association, vol. 69, no. 11, 2019, pp. 1312–1330., https://doi.org/10.1080/10962247.2019.1668497.

EPA NEI (National Emissions Inventory v1): Air Pollutant Emission Trends Data, available at: http://www.epa.gov/ttn/chief/trends/index.html last access: 23 June 2015.

Farris, Betsy M., et al. "Demonstration of an off-Axis Parabolic Receiver for near-Range Retrieval of Lidar Ozone Profiles" Atmospheric Measurement Techniques, vol. 12, no. 1, 2019, pp. 363–370., https://doi.org/10.5194/amt-12-363-2019.

Gelaro, Ronald, et al. "The Modern-Era Retrospective Analysis for Research and Applications, Version 2 (Merra-2)." Journal of Climate, vol. 30, no. 14, 2017, pp. 5419–5454., https://doi.org/10.1175/jcli-d-16-0758.1.

Gronoff, Guillaume, et al. "A Method for Quantifying near Range Point Source Induced O3 Titration Events Using Co-Located Lidar and Pandora Measurements." Atmospheric Environment, vol. 204, 2019, pp. 43–52., https://doi.org/10.1016/j.atmosenv.2019.01.052.

Gronoff, G; Berkoff, T; Knowland, KE; Lei, L; Shook, M; Fabbri, B; Carrion, W; Langford, AO; "Case study of stratospheric Intrusion above Hampton, Virginia: lidar-observation and modeling analysis", Atmospheric Environment,118498, 2021, Pergamon

Han, Jiawei, et al. Data Mining Concepts and Techniques. Morgan Kaufmann, 2011.

Hu, L., Keller, C. A., Long, M. S., Sherwen, T., Auer, B., Da Silva, A., et al. (2018). Global simulation of tropospheric chemistry at 12.5 km resolution: Performance and evaluation of the GEOS-Chem chemical module (v10-1) within the

NASA GEOS Earth system model (GEOS-5 ESM). Geoscientific Model Development, 11, 4603-4620. https://doi.org/10.5194/gmd-11-4603-2018.

Kaufman, L. & Rousseeuw, P. (1990). Finding groups in data: An introduction to cluster analysis.

Keller, Christoph A., et al. "Description of the NASA Geos Composition Forecast Modeling System GEOS-CF v1.0." Journal of Advances in Modeling Earth Systems, vol. 13, no. 4, 2021, https://doi.org/10.1029/2020ms002413.

Knowland, K.E., Keller, C.A., Lucchesi, R., 2019. 'File specification for GEOS-CF products', GMAO office note No. 17 (version 1.0). available from: https://gmao.gsfc.nasa.gov/pubs/office_notes.php, 32.

Knowland, K. Emma, et al. "NASA GEOS Composition Forecast Modeling System GEOS-CF v1.0: Stratospheric Composition." 2021, https://doi.org/10.1002/essoar.10508148.1.

Lawson, Richard G., and Peter C. Jurs. "New Index for Clustering Tendency and Its Application to Chemical Problems." Journal of Chemical Information and Computer Sciences, vol. 30, no. 1, 1990, pp. 36–41., https://doi.org/10.1021/ci00065a010.

Leblanc, Thierry, et al. "Validation of the TOLNet lidars: the Southern California Ozone Observation Project (SCOOP)." Atmospheric measurement techniques 11.11 (2018): 6137-6162.

Lei, Liqiao; Berkoff, Timothy A; Gronoff, Guillaume P; Su, Jia; Nehrir, Amin R; Wu, Yonghua; Moshary, Fred; Kuang, Shi; "Retrieval of UVB aerosol extinction profiles from the ground-based Langley Mobile Ozone Lidar (LMOL) system", Atmospheric Measurement Techniques Discussions, 1-22,2021, Copernicus GmbH

Li, Wei, et al. "Identification of Sea Breeze Recirculation and Its Effects on Ozone in Houston, TX, during Discover-Aq 2013." Journal of Geophysical Research: Atmospheres, vol. 125, no. 22, 2020, https://doi.org/10.1029/2020jd033165.

McDuffie, Erin E., et al. "A Global Anthropogenic Emission Inventory of Atmospheric Pollutants from Sector- and Fuel-Specific Sources (1970–2017): An Application of the Community Emissions Data System (CEDS)." Earth System Science Data, vol. 12, no. 4, 2020, pp. 3413–3442., https://doi.org/10.5194/essd-12-3413-2020.

Orbe, Clara, et al. "Large-Scale Atmospheric Transport in GEOS Replay Simulations." Journal of Advances in Modeling Earth Systems, vol. 9, no. 7, 2017, pp. 2545–2560., https://doi.org/10.1002/2017ms001053.

Ring, Allison M., et al. "Evaluating Commercial Marine Emissions and Their Role in Air Quality Policy Using Observations and the CMAQ Model." Atmospheric Environment, vol. 173, 2018, pp. 96–107., https://doi.org/10.1016/j.atmosenv.2017.10.037.

Stauffer, Ryan M., et al. "Characterizing Global Ozonesonde Profile Variability from Surface to the UT/Ls with a Clustering Technique and MERRA-2 Reanalysis." Journal of Geophysical Research: Atmospheres, vol. 123, no. 11, 2018, pp. 6213–6229., https://doi.org/10.1029/2018jd028465.

Strode, Sarah A., et al. "Global Changes in the Diurnal Cycle of Surface Ozone." Atmospheric Environment, vol. 199, 2019, pp. 323–333., https://doi.org/10.1016/j.atmosenv.2018.11.028.

https://doi.org/10.5194/acp-2022-133
Preprint. Discussion started: 23 March 2022


Atmospheric Chemistry and Physics Discussions

Sullivan, J. T., et al. "Optimization of the GSFC Tropoz Dial Retrieval Using Synthetic Lidar Returns and Ozonesondes – Part 1: Algorithm Validation." Atmospheric Measurement Techniques, vol. 8, no. 10, 2015, pp. 4133–4143., https://doi.org/10.5194/amt-8-4133-2015.

Sullivan, John T., et al. "Results from the NASA GSFC and LARC Ozone Lidar Intercomparison: New Mobile Tools for Atmospheric Research." Journal of Atmospheric and Oceanic Technology, vol. 32, no. 10, 2015, pp. 1779–1795., https://doi.org/10.1175/jtech-d-14-00193.1.

Thompson, Anne M., et al. "Ozone Profiles in the Baltimore-Washington Region (2006–2011): Satellite Comparisons and Discover-AQ Observations." Journal of Atmospheric Chemistry, vol. 72, no. 3-4, 2014, pp. 393–422., https://doi.org/10.1007/s10874-014-9283-z.

Torgo, Luís. "Data Mining with R." Chapman & Hall/CRC Data Mining and Knowledge Discovery Series, 2010, https://doi.org/10.1201/b10328.

Wang, Lihua, et al. "Quantifying Tolnet Ozone Lidar Accuracy during the 2014 Discover-AQ and Frappé Campaigns." Atmospheric Measurement Techniques, vol. 10, no. 10, 2017, pp. 3865–3876., https://doi.org/10.5194/amt-10-3865-2017.

Wu, Yonghua; Nehrir, Amin R; Ren, Xinrong; Dickerson, Russell R; Huang, Jianping; Stratton, Phillip R; Gronoff, Guillaume; Kooi, Susan A; Collins, James E; Berkoff, Timothy A; "Synergistic aircraft and ground observations of transported wildfire smoke and its impact on air quality in New York City during the summer 2018 LISTOS campaign", Science of The Total Environment, 773,145030, 2021, Elsevier.